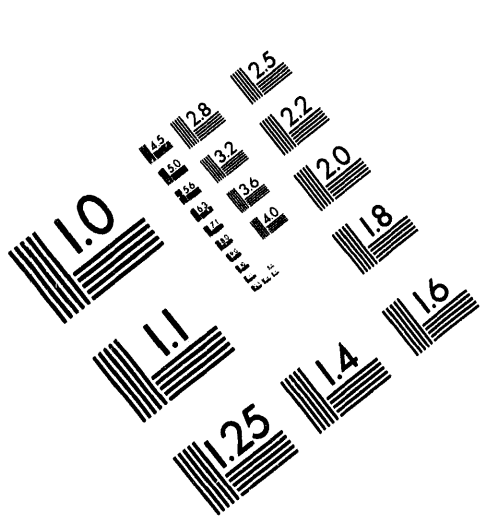

Association for Information and Image Management
1100 Wayne Avenue, Suite 1100
Silver Spring, Maryland 20910
301/587-8202

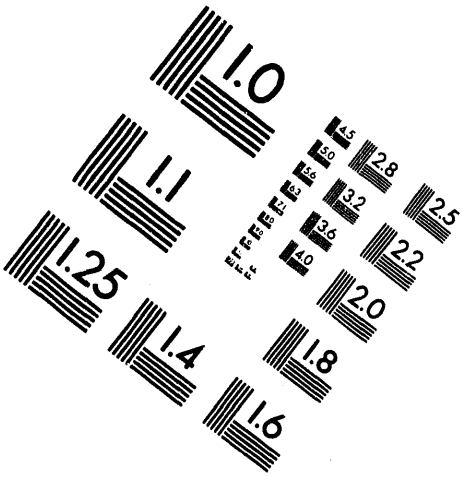

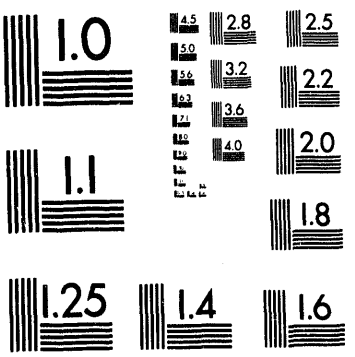

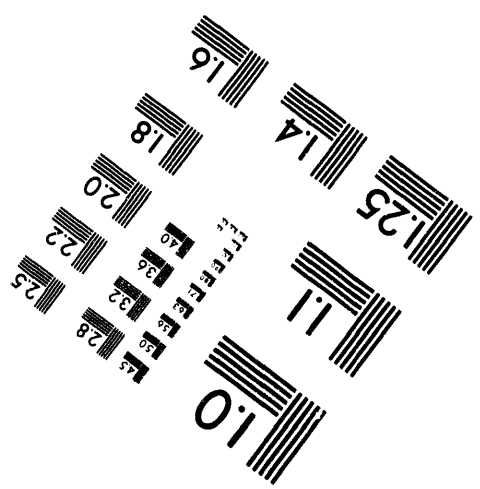

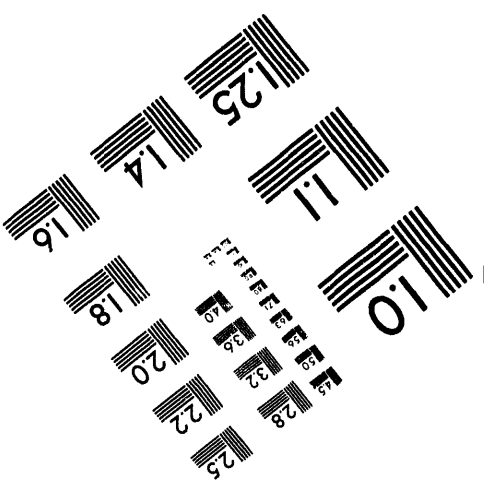

1 of 1

LA-UR -93-4416

Los Alamos National Laboratory is operated by the University of California for the United States Department of Energy under contract W-7405-ENG-36

TITLE: MODELING FRACTURE IN CEMENTED GRANULAR MATERIAL

AUTHOR(S): B.C. Trent
L.G. Margolin

SUBMITTED TO: Application of Fracture Mechanics to Geomaterials
ASCE Geotechnical Special Publications
ASCE Annual Meeting
October 6-13, 1994
Atlanta, Georgia

DISCLAIMER

Los Alamos National Laboratory
Los Alamos, New Mexico 87545

Modeling Fracture in Cemented Granular Material

B.C. Trent [1] and L.G. Margolin [2]

Abstract

We have conducted an extensive study to determine the underlying physical processes that govern inelastic behavior in brittle geologic materials. The distinct element method has been used to perform many different numerical experiments to help understand how permanent macroscopic deformations can be characterized in terms of microscopic parameters, such as fracture of the binding material and the topology of the granular matrix. In particular, we have constructed a distinct element model of a cemented granular material which accounts for the elastic forces due to bonding between pairs of spherical particles, and which allows for the possibility of anisotropic damage to the bonds due to the growth of small brittle cracks within the bonds. We then develop a general constitutive theory that estimates the effective elastic moduli of a cemented granular material by applying statistical mechanical averaging to a purely micromechanical model. In this paper, we use the numerical model to validate the predictions of the theory for various prescribed patterns of damage. Specifically, we impose several anisotropic patterns of damage on the bonds of a randomly generated assembly of particles. We then do numerical experiments, sending both p-waves and s-waves through samples and measuring the wave velocities. The predictions of the theory for these velocities agree well with the results of the numerical model for a variety of damage patterns. We discuss the implications of our theory, as well as potential applications.

Introduction

Constitutive models for geologic materials have traditionally been built around phenomenological models based on plasticity. These are relatively easy to implement and can usually be modified to fit virtually any experimental data obtained in the laboratory. Unfortunately, they are not based on physical mechanisms, so their applicability to different classes of problems is quite limited. The issue of scale is always a problem and strain rate dependencies usually add another layer of

[1] Applied Theoretical Physics Division, Los Alamos National Laboratory, Los Alamos NM 87544; e-mail BCT@LANL.GOV

[2] Institute for Geophysics and Planetary Physics, Los Alamos National Laboratory, Los Alamos NM 87544; e-mail LEN@LANL.GOV

complexity, which compounds the difficulty of relating the model parameters to anything physical. Our goal has been to develop a general constitutive model, which is applicable to quasistatic and dynamic problems without regard to scale, and which depends on parameters that can be measured directly in the laboratory. In order to work toward this goal, it has been necessary to study in great detail the granular-level mechanisms that govern macroscopic inelastic behavior in the aggregate solids of interest. We have utilized the concept of a numerical laboratory to "observe" and measure the mesoscale parameters which would not ordinarily be available in a physical laboratory. The numerical tool used for the testbed is the distinct element method. We have incorporated linear elastic fracture mechanics as a damage mechanism within the interparticle bonding. Much of our early work was devoted to refining the distinct element code and performing representative and realistic calculations which are summarized below. More recently, our efforts have concentrated on developing a constitutive model to be used in large-strain continuum codes. The distinct element method was used to test the analytic model. These results are discussed the later sections of the paper. This research has provided some insight into the fundamental cause of inelastic behavior in cemented granular material and outlines a framework for a new class of constitutive model to help solve complex boundary value problems.

Background

In this paper we continue our development and validation of a constitutive theory for a cemented granular material at high strain rate. Our goal is to construct a model that can reproduce the complex behavior of such materials and yet is simple enough to use in large-scale numerical simulations of solid continuum dynamics. To ensure proper scaling with the various physical parameters, we have based our model on a microphysical description of a granular material rather than on macroscopic plasticity [Margolin, 1984]. Furthermore, to validate our analysis and its assumptions, we have constructed a numerical model based on the Discrete Element Method (DEM) [Cundall, 1987].

Our microphysical description of a granular material is based on two premises. First we assume that the elastic properties -- i.e., the effective elastic moduli -- of a cemented granular material depend mostly on the elastic properties of the bonding material and on the topology of the bonding, but are relatively independent of the properties of the grains. Of course other properties of the material, such as bulk density, may depend mostly on the grains. Second we assume that macroscopic inelasticity in the response of a cemented granular material to loading under high strain rate is mostly due to one microphysical process, the fracture of preexisting bonds. By fracture, we mean the growth of small brittle cracks within the bonds that weaken and eventually sever the bonds.

We have formulated a computer model of a cemented granular material using the Discrete Element Method [Trent, 1988; Trent and Margolin, 1992a] and based on the premises of the preceding paragraph. In particular we modified the TRUBAL code [Cundall, 1987] by adding elastic bonds between pairs of spherical particles whose centers are closer than a specified distance. Although forces and moments may still be produced by direct particle-particle contacts, the behavior of our simulated granular material is actually dominated by the forces and moments produced by the stretching or shearing of the bonds as the particles rotate and/or get closer or farther apart. In addition, we have embedded tiny brittle cracks within each of the bonds. Such a crack may grow when the stresses within the bond exceed a growth criterion [Griffith, 1920]. The restoring force of a bond is found to be proportional to the uncracked cross-sectional area, and so is reduced as the crack grows. In a general

external stress field, the stress within a bond is a function of the bond orientation. Thus most generally, the size of the embedded crack will be a function of the bond orientation as well as the history of loading. Macroscopically, we refer to the general property of anisotropic crack growth as damage.

Our DEM model represents a considerable simplification of a real cemented granular material. In particular, one might question whether fracture within the bonds (the only mechanism that we have provided for inelasticity) can reproduce the complex behavior of real granular materials, which ranges from brittle to quasibrittle to ductile. In previous work the model has been used to reproduce such qualitative behavior as macroscopic fracture [Trent and Margolin, 1992a] as well as plasticity in the collapse of hollow spheres [Trent, 1987]. On the other hand, the DEM model is not suited for simulations of problems on length scales like tens and hundreds of meters. This is because the number of grains represented would overwhelm today's computers both in terms of CPU and memory requirements. Moreover, most of the detailed output of such a calculation would be useless. Such problems are more easily solved with continuum codes that contain a realistic constitutive law for the behavior of granular materials.

The construction and implementation of such a realistic constitutive law is the ultimate goal of our research. We begin this paper with a brief description of the numerical model. Then we will review our theoretical approach, including previous work we have done to validate the model in the case of isotropic damage. We also discuss how the theory may be used to create a constitutive model, which emphasizes the importance of being able to accurately treat anisotropic damage. Finally we present results of an extensive numerical study of the effective elastic moduli of material with prescribed damage patterns and compare these results with the predictions of our theory.

The Numerical Model

The distinct element model TRUBAL assumes a system of spherical rigid particles. We have constrained the motion for our study to only two dimensions. We have modified this model by adding elastic bonds between certain pairs of particles whose centers are closer than some specified distance. Within each bond, we have placed a two-dimensional Griffith crack, whose normal is oriented perpendicular to the line joining the particle centers. The geometry of the bonding is described by three dimensionless parameters -- α, β, and δ -- that are illustrated in Fig. 1.

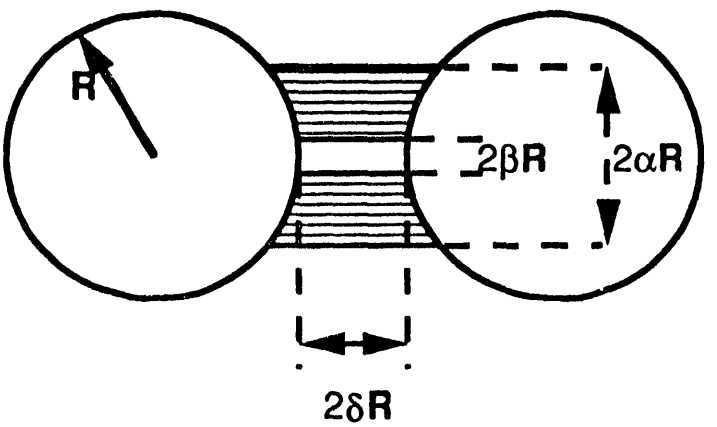

Figure 1. The dimensionless parameters α,β, and δ define the geometry of bonded grains. In the middle of the bond is a vertical crack.

The total bond width is α,the width of the Griffith crack is β, and δ is the length of the bond. Each of these parameters is nondimensionalized by the particle radius R.

Under loading, the particles are displaced relative to each other. The restoring forces and moments that are applied to each bonded particle pair are based on analytic equations developed for the three independent modes of deformation: simple tension or compression in which the bonded particles move toward or away from each other; rolling torsion in which the two particles rotate in opposite directions; and shearing torsion in which both particles rotate in the same direction. The form of the restoring stiffness for simple tension/compression is given, for example, in Eq. 1.

$$\frac{F/\Delta u}{E} = -w + \frac{a}{\sqrt{a^2-1}}\left(\frac{a\cos(w)-1}{a-\cos(w)}\right)\Bigg| \begin{matrix} w=\sin^{-1}(\alpha) \\ w=\sin^{-1}(\beta) \end{matrix} \qquad (1)$$

where α, β and δ ($a = 1+\delta$) are defined in Fig. 1. The restoring force of the bond on the particle is F and Δu is the incremental stretching of the bond. The details of the derivations of the analytic expressions can be found in Trent [1987] and Trent [1988].

A number of calculations have been performed where crack growth has dominated the numerical results. These have included stress wave-induced surface spall [Trent, 1986], compaction (P-α conceptual model) of bonded particles in a spherical geometry with a central void [Trent, 1986], and a study of initial flaw size on macroscopic tensile strength [Trent and Margolin, 1992a]. Since the forces in the bonding material are modeled explicitly, the stresses are easily calculated The generalized criterion for crack growth in Eq. 2 has been incorporated into the code [Margolin, 1984b].

$$\sigma_n^2 + \frac{\sigma_s^2}{2(1+\nu)} \geq \frac{\pi T E}{2(1-\nu^2)\, c} \qquad (2)$$

where σ_n is the normal stress in the bond, σ_s is the shear stress in the bond, ν is the Poisson's ratio of the bonding material, T is the energy required to build a new fracture surface, E is the elastic modulus of the bonding material and c is the current fracture length in the bond. Subcycling was incorporated in the code to ensure exact compatibility within a time step between the imposed strain conditions on the bonding and the stiffness reduction resulting from fracture at a finite rate. The details of the implementation of this procedure are given elsewhere [Trent, 1986; Trent, 1988].

The primary predictions of our analytic model are the effective elastic moduli. Although these can be measured directly in the numerical model, it turns out to be easier to infer them from the wave speeds measured in numerical wave propagation experiments. For example, we generate tensile waves by giving the particles along the bottom edge of the sample a constant downward velocity for a short time. Their velocity is then set to zero and the resulting ringing recorded. The time history of the particle velocities within the sample determines the transit time of the wave across the sample. Knowing the size of the sample, it is then possible to calculate the p-wave velocity.

By applying a horizontal velocity to the particles on the bottom boundary, one can similarly generate a shear wave and thus measure the s-wave velocity, normal to the particle velocity. For an isotropic material, these two velocities are sufficient to

determine the material Poisson's ratio, as well as the ratio of Young's modulus to bulk density. Details of this procedure can be found in Trent and Margolin [1992a].

A key stage in the derivation of our analytic model will be the "average particle" assumption, which implies the statistical homogeneity of the sample. There are at least two sources of inhomogeneity in the numerical model -- the presence of boundaries, and biases due to the method of sample preparation. The effects of the boundaries can be lessened by increasing the number of particles in the numerical sample. In previous studies [Trent and Margolin, 1992b] our samples typically contained about 300 particles. In the present study, we have increased this number to over 1000.

We form our numerical samples by allowing the particles to settle under gravity, and then bonding all particles whose centers are closer than some specified distance. This process is designed to yield a more realistic sample, but does introduce anisotropy due to the preferred direction of gravity. This source of anisotropy will not decrease as the number of particles is increased. In [Trent and Margolin, 1992b] we estimated the size of this effect to construct error bars for our numerical results.

Micromechanical Model

The micromechanical model that underlies our constitutive law is an idealization of our discrete element model. It also consists of an assembly of two-dimensional grains of radius R. Grains which are closer than some specified distance are considered to be bonded to each other. As in the numerical model, when the particles are displaced from their equilibrium positions, restoring forces result.

The macroscopic stress can be defined in terms of these forces [Margolin and Trent, 1990]

$$\bar{\sigma}_{ij} = \frac{2}{V} \sum_{\text{particles}} \sum_{a} F_i^{(a)} L_j^{(a)} \qquad (3)$$

Here the inner sum is over the contacts of a particular particle. By contact, we mean the connection between a particle and a bond. The superscript (a) identifies the contact. **F** is the force within the bond. **L** is the vector pointingfrom the contact

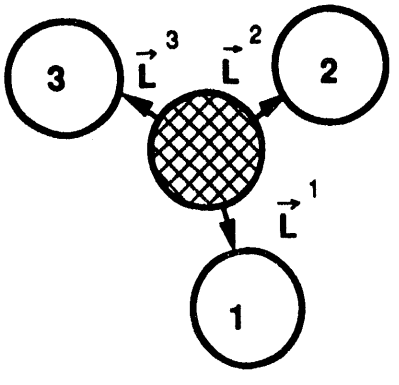

Figure 2. A specific configuration of a central particle bonded to three neighbors.

along the bond, and with magnitude equal to half of the length of the bond (i.e., $|\delta R|$; see Fig. 1). V is the volume of the sample. A specific realization of a central particle and its bonds is shown in Fig. 2.

Equation 3 is an exact relation between the macroscopic stress field and the microscopic forces. However it requires a complete and detailed knowledge of the configuration of the particles and the bonds. Such details are of course available in the numerical model. However to construct our constitutive theory, we will simplify this equation by replacing the inner sum over the contacts about a particular particle by a sum over the contacts of an "average" particle. The outer sum over all the particles is then just the total number of particles, N, times the inner sum over the average particle.

To be more precise about what we mean by an "average" particle, let us assume that we can write down a probability distribution for the number of neighbors to which a central particle is bonded, and for the lengths and orientations of the individual bonds. We denote this distribution

$$P\ (N_a, L^{(1)}, L^{(2)}, \ldots L^{(N_a)}) \tag{4}$$

where N_a is the number of neighbors. Thus the distribution P represents the probability of any possible configuration of neighbors and bonds around a particle. In these terms we can rewrite Eq. 3

$$\bar{\sigma}_{ij} = \frac{2N}{V} < \sum_{a=1}^{N_a} F_i^{(a)} L_i^{(a)} > \tag{5}$$

The brackets mean the distribution P is used to average over all configurations.

The next step in the development of our theory is to write the force F in terms of the bond orientation vectors L and the applied strain tensor. The final result is

$$\bar{\sigma}_{ij} = \frac{2\rho E_b \bar{L}}{\pi R \rho_\mu} < \sum_{a=1}^{Na} \tau_j^{(a)} \tau_j^{(a)} \tau_k^{(a)} \tau_m^{(a)}\ (\alpha^{(a)} - \beta^{(a)}) > \bar{\varepsilon}_{km} \tag{6}$$

where ρ is the bulk density of the granular material, ρ_μ is the density of the grains themselves, and E_b is the Youngs' modulus of the bond material. The vector τ is the unit vector in the direction of the bond -- i.e., ($\cos\theta$, $\sin\theta$). To derive this form, we have assumed that the bond length is uncorrelated with the bond orientation. Details of the derivation can be found in Margolin and Trent [1992].

Review of Previous Validation Studies

We begin by noting that an expression for the effective elastic moduli can be written down from Eq. 6 and the definition

$$M_{ijkm} \equiv \frac{\partial \bar{\sigma}_{ij}}{\partial \bar{\varepsilon}_{km}} \tag{7}$$

so

$$M_{ijkm} = \frac{2\rho E_b \bar{L}}{\pi R \rho_\mu} < \sum_{a=1}^{N_a} \tau_i^{(a)} \tau_j^{(a)} \tau_k^{(a)} \tau_m^{(a)}\ (\alpha^{(a)} - \beta^{(a)}) > \tag{8}$$

The dependence of the moduli on the Young's modulus E_b of the bond material is consistent with our assumption that only the elastic properties of the bond matter and then from dimensional analysis. This dependence, as well as the dependence on bulk density, was verified using the DEM code [Trent and Margolin, 1992a].

The term in the angular brackets is more difficult to treat. We begin by assuming that the orientations of the bonds are not correlated. Strictly speaking this cannot be so, since the bonds cannot physically overlap; that is, there is a small angle about the position of each bond from which all other bonds are excluded. However this assumption should be adequate when there are relatively few bonds around the particle. In this case, the sum over "a", the bond index, becomes just the coordination number N_a times the bracket for any one bond. Then the effective moduli should scale directly with average bond length, and with the expected value of the coordination number. These scalings were verified [Margolin and Trent, 1990].

If one further assumes that the bonds, *as well as any damage*, are isotropically distributed, then the angular integrals can be evaluated and the actual values of the moduli predicted. Some examples are provided in the appendix. These calculations were also performed [Margolin and Trent, 1990] and showed excellent agreement as long as the expected value of the coordination number was small. In the numerical model, we control the degree of bonding by specifying the maximum separation between bonded particles. For example, when we specify that all grain pairs for which $\delta \leq .4$ (see Fig. 1) are bonded, then the expected coordination number $< N_a > = 3.3$. When we increase maximum bonding distance to $\delta \leq 1.0$, we find $< N_a > = 4.5$. We found systematic and significant differences between the code and the theory for $\delta > 1.0$, with the theory predicting the larger moduli.

It turns out to be possible to account for these differences by enforcing the physical constraint that the bonds cannot overlap. In estimating the angular integral, for example for the second bond, we exclude a small angle of $\pm \psi$ about the orientation of the first bond. This does not alter the probability function for the orientation of a single bond (which we continue to assume is isotropic), but rather for the probability function of two or more bonds. That is, originally we had assumed that the bonds' orientations were not correlated. Now we introduce a small anti-correlation. This correction is described in [Margolin and Trent, 1992] where we evaluate the changes in the angular integrals using a perturbation theory. With this correction, the agreement between theory and the DEM code is excellent for all values of the maximum bonding distance $2\delta R$.

To summarize then, we have validated our theoretical expression for the effective moduli Eq. 8 for isotropic materials. In this paper, we will extend our studies to anisotropic materials. We will motivate the importance of this step in the next section before showing new comparisons.

Constitutive Theory and Anisotropic Damage

The main purpose of this paper is to validate the formulae for the effective elastic moduli for nonisotropic materials. Anisotropy may be a material property, due to the detailed history of the formation of the bonds. However anisotropy due to inelastic changes (i.e., crack growth within the bonds) is of greater interest here. The reason for our interest lies in the way we expect to couple our constitutive model into a solid dynamics code.

Solid dynamics codes solve numerically the time-dependent partial differential equations that express the conservation of mass, momentum, and energy. In the simplest case (in which one ignores the energy equation), the solution procedure is a cyclic process:

1) the divergence of the stress tensor is used to update the velocity field;
2) the velocity field is used to calculate the strain rate tensor;
3) the strain rate tensor is used by the constitutive law to update the stress tensor.

Within the constitutive law, the damage, e.g., the crack width function $\beta(\theta)$ in Eq. 8, appears as an internal variable. The constitutive law has the following components:

1) the current damage is used to calculate the effective elastic moduli;
2) the moduli and the strain rate tensor are used to update the stress tensor;
3) the stress tensor is used to update the damage based on Griffith's law.

Thus, in addition to updating the stress field, the constitutive law must also update the crack width function $\beta(\theta)$, which will depend in a complicated way on the history of loading. The important feedback from the damage is in its effect on the elastic moduli, which is what we want to validate.

In the following section, we will compare DEM predictions of the moduli with the theory, for *specified* crack width functions. For a general loading history, the function $\beta(\theta)$ will not be representable in analytic form. However for any given stress field, Griffith's law defines a critical axis and a critical angle. Bonds whose orientations lie within the cone defined by this axis and angle are unstable to crack growth. With this in mind, we have attempted to choose damage patterns for our comparison that are similar to what might appear in actual geologic conditions.

Comparisons of the Theory and the Analytic Model

Our purpose in this section is to validate Eq. 8. We will do this by specifying various patterns of damage in the material. Insofar as the analytic theory is concerned, all that changes are the angular integrals within the brackets. Furthermore, the longitudinal speed is proportional to the square root of the modulus M_{1111}, whereas the shear wave speed is proportional to the square root of M_{1212}, with the same constant of proportionality. Thus the theory predicts that each of the wave speeds measured in the DEM experiments (described below) divided by the square root of the appropriate angular integral should be a constant.

Of course the randomly generated DEM sample is not exactly isotropic. The particular realization that we have used contains 1042 particles and 2906 bonds. The distinct element assembly is shown in Fig. 3 where the straight line indicates a bond connecting two particles. Figure 4 shows the orientations of these bonds sorted into eighteen bins, each ten degrees wide. We find that there is a standard deviation of the order of ten percent from the average value of 161.4 bonds/bin. Since the actual number of bonds in a bin represents a weight in the angular integrals that should be constant and since the deviations are distributed fairly isotropically, one might expect to see deviations between the theory and the DEM experiments of the same order.

We have investigated two different damage patterns. In case 1, the current crack length of each bond varies continuously from horizontal to vertical as follows:

$$\beta = \beta_0 + \beta_1 \cos^2(\theta + \phi) \qquad (9)$$

where β_0 is the minimum fracture length
$\beta_0 + \beta_1$ is the maximum fracture length
θ is the orientation of the bond measured from the horizontal
ϕ is a constant angle that specifies the orientation of the damage distribution

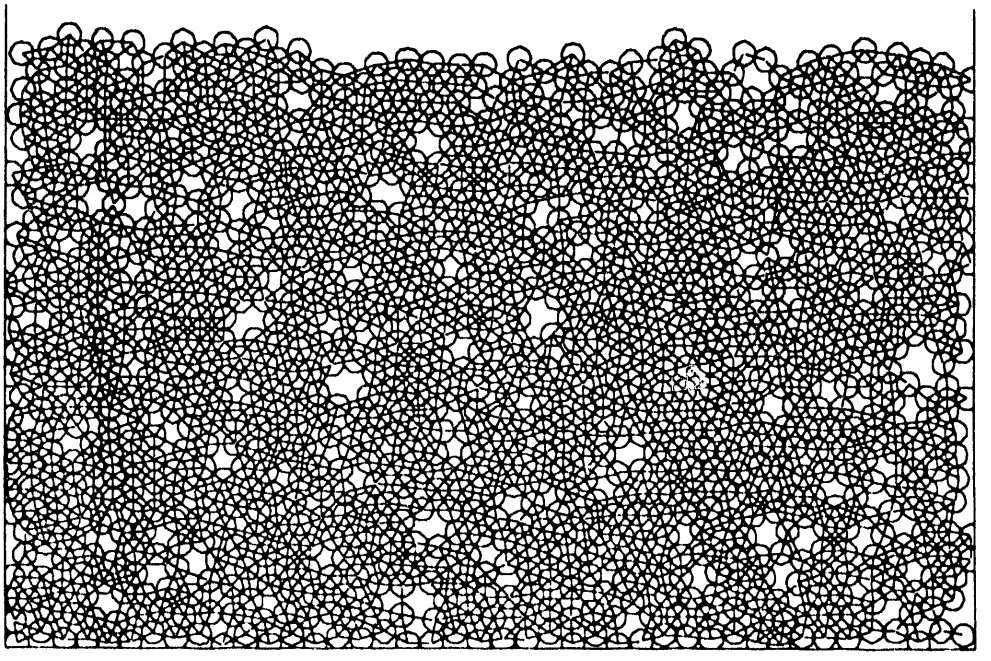

Figure 3. Distinct element assembly with 1024 particles and 2906 bonds.

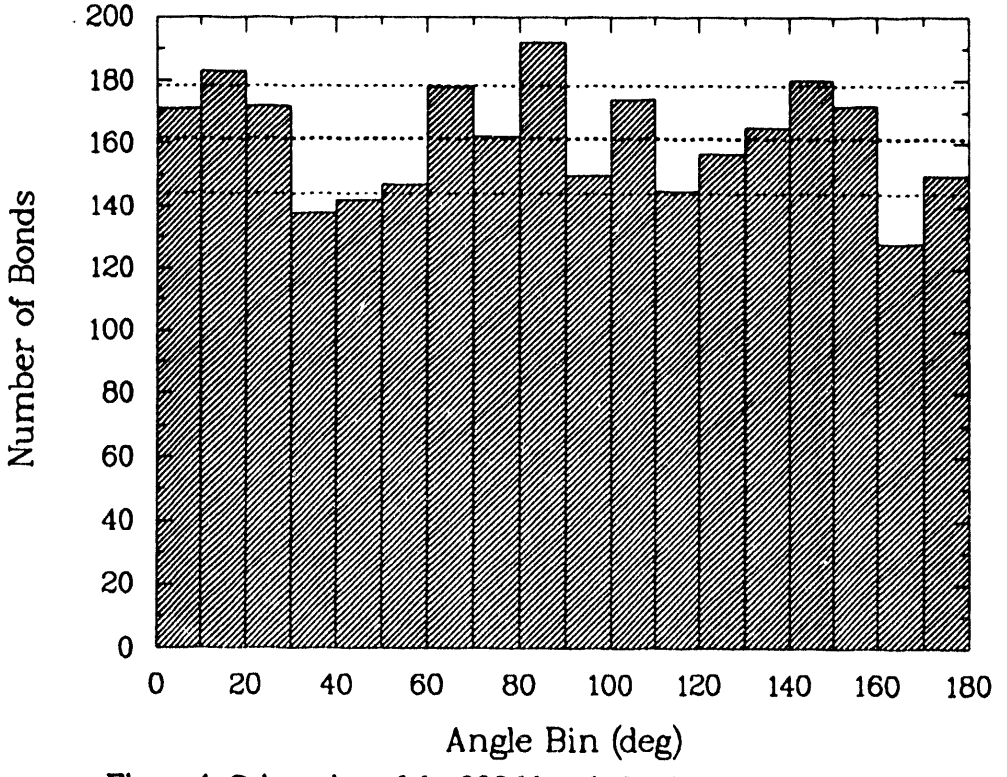

Figure 4. Orientation of the 2906 bonds for the sample shown in Fig. 3. Zero and 180 degrees are aligned with the vertical axis.

We illustrate this distribution in Fig. 5, choosing as the parameters $\beta_0 = 0.05$, $\beta_1 = 0.40$ and $\phi = 0^o$. In all cases we have chosen $\alpha = 0.50$. It is clear that for this choice of parameters, most of the intact bonds are nearly vertical. In Fig. 6 we show the distribution for the same choice of parameters, except that $\phi = 90^o$. In this case, the more intact bonds are nearly horizontal. We emphasize that for both cases, and indeed for all the numerical simulations, the samples (as defined by the total number of particles, bonds and their detailed orientations) are identical. Only the damage patterns are varied. Recall from Eq. 1 that the stiffness of a given bond depends not only on the damage, β, but also on the separation distance, δR, which is different for each bond. Bonds with smaller separations are stiffer, since a given incremental strain will cause higher stresses in the bonding material. When $\beta_1 = 0$, we have an isotropic distribution of damage. In this case, the standard deviation about the numceical results is quite small. When $\beta_1 \neq 0$, we show several anisotopic distributions. In these cases, the standard deviation is larger, but still is only about 7% of the mean, consistent with the angular distribution of bonds. The results for a suite of runs is shown in Table 1. In this table, the column labeled form factor is derived by dividing the measured speed by the square root of the angular integral. The wave type refers to longitudinal (p) or shear (s) loading. The solutions of the angular integrals for both p-wave and s-wave loading are in the appendix.

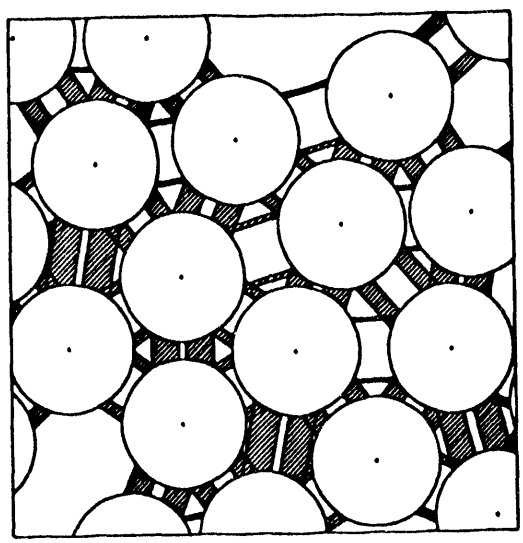

Figure 5. Representation of bonds for case 1 where the orientation angle, ϕ, is zero. Note the less damaged bonds are vertical.

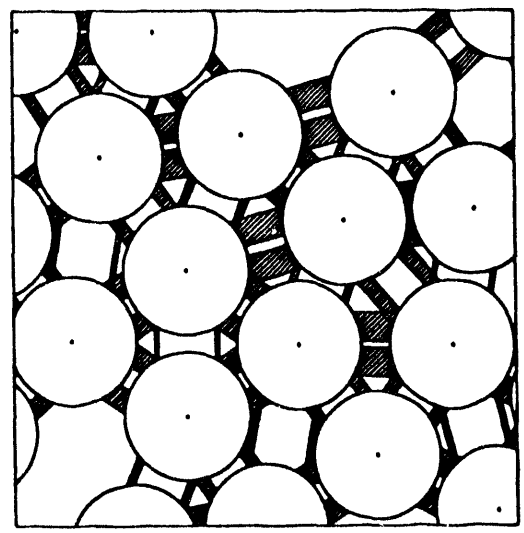

Figure 6. Representation of bonds where ϕ is $\pi/2$. Note the more intact bonds are now horizontal.

In case 2, the damage is defined

$$\begin{aligned} \beta &= \beta_0 \quad \text{for } \theta > \phi \text{ or } \theta < -\phi \\ \beta &= \beta_1 \quad \text{for } \phi > \theta > -\phi \end{aligned} \tag{10}$$

Here the sample has only two levels of damage, β_0 and β_1. The damage of any particular bond depends on its orientation, θ, and the angle ϕ which defines the orientation where the damage changes from β_0 to β_1. The results of the case 2 studies are given in Table 2. These results are qualitatively similar to those of case 1, with standard deviations which are only 6% of the mean. Again, the angular integrals are evaluated for this case for both p and s-waves in the appendix.

Table 1. Summary of Distinct Element Results for Case 1 (α=0.50 for all cases)

Wave Type	β_0	β_1	ϕ	Mean β / α	Measured Speed (m/s)	Angular Integral	Form Factor, K
p	0.05	0.00		0.1000	1882.7	0.2651	3656.59
s	0.05	0.00		0.1000	1159.7	0.0884	3900.49
p	0.10	0.00		0.2000	1728.3	0.2356	3560.67
s	0.10	0.00		0.2000	1042.5	0.0785	3720.84
p	0.25	0.00		0.5000	1286.4	0.1473	3351.77
s	0.25	0.00		0.5000	779.2	0.0491	3516.48
p	0.05	0.40	0.0	0.5045	1530.5	0.2258	3220.86
s	0.05	0.40	0.0	0.5045	734.8	0.0491	3316.11
p	0.05	0.40	90.0	0.4955	964.0	0.0687	3677.89
s	0.05	0.40	90.0	0.4955	689.0	0.0491	3109.41
p	0.05	0.30	0.0	0.4034	1619.3	0.2356	3336.10
s	0.05	0.30	0.0	0.4034	860.7	0.0589	3546.45
p	0.05	0.30	90.0	0.3966	1212.5	0.1178	3532.72
s	0.05	0.30	90.0	0.3966	815.2	0.0589	3358.97
p	0.15	0.35	0.0	0.6539	1251.6	0.1718	3019.63
s	0.15	0.35	0.0	0.6539	558.1	0.0344	3009.07
p	0.15	0.35	90.0	0.6461	556.4	0.0344	2999.91
s	0.15	0.35	90.0	0.6461	522.7	0.0344	2818.21

The form factors for all cases in Tables 1 and 2 are shown in Fig. 7. Note the variation in values is of the same order as the variation in bond orientation shown in Fig. 4. An earlier suite of identical calculations was performed on a smaller assembly of only 270 particles, glued together with 610 bonds. The bond porosity (not counting the volume of the bonds) of this assembly was 38%, compared to 26% for the assembly shown in Fig. 3. Higher porosity samples will have lower acoustic speeds. The standard deviation of bond orientations was over 20% of the mean, compared to only 10% for the bigger assembly. Even though these differences in sample characteristics are significant, the form factors for this case are quite similar, as illustrated in Fig. 8. Notice the mean (thick dashed line) is nearly the same as in Fig. 7 but the variation is greater, reflecting the greater variation in nonisotropic bond orientation.

To summarize, recall that both case 1 and case 2 consisted of strongly vertically as well as strongly horizontally oriented damage subjected to longitudinal and shear loading. We see that the form factors predicted by both the results from the case 1 anisotropic damage studies, and the case 2 anisotropic damage studies are consistent with the data derived from isotropic damage studies. Furthermore the standard deviations derived from each of the two data sets are only about 7% of the mean, and are consistent in magnitude with the anisotropy of the distribution of bond orientations in the numerical sample.

Table 2. Summary of Distinct Element Results for Case 2 (α=0.50 for all cases)

Wave Type	β_0	β_1	ϕ	Mean β / α	Measured Speed (m/s)	Angular Integral	Form Factor, K
p	0.05	0.40	45.0	0.4517	1603.2	0.2495	3209.61
s	0.05	0.40	45.0	0.4517	761.3	0.0540	3276.11
p	0.40	0.05	45.0	0.4483	959.2	0.0745	3514.24
s	0.40	0.05	45.0	0.4483	678.8	0.0540	2921.09
p	0.05	0.40	60.0	0.5649	1384.7	0.2129	3001.01
s	0.05	0.40	60.0	0.5649	646.3	0.0331	3552.39
p	0.40	0.05	30.0	0.5589	850.5	0.0613	3435.14
s	0.40	0.05	30.0	0.5589	585.7	0.0331	3219.30
p	0.05	0.30	45.0	0.3512	1690.6	0.2539	3355.13
s	0.05	0.30	45.0	0.3512	895.7	0.0638	3546.11
p	0.30	0.05	45.0	0.3488	1253.7	0.1289	3491.94
s	0.30	0.05	45.0	0.3488	836.5	0.0638	3311.74
p	0.05	0.30	60.0	0.4321	1538.0	0.2278	3222.40
s	0.05	0.30	60.0	0.4321	837.9	0.0489	3789.11
p	0.30	0.05	30.0	0.4278	1176.3	0.1195	3402.78
s	0.30	0.05	30.0	0.4278	772.8	0.0489	3494.72
p	0.15	0.35	45.0	0.5010	1448.0	0.1973	3259.91
s	0.15	0.35	45.0	0.5010	789.4	0.0491	3562.51
p	0.35	0.15	45.0	0.4990	1077.7	0.0973	3454.95
s	0.35	0.15	45.0	0.4990	718.3	0.0491	3241.64
p	0.15	0.35	60.0	0.5657	1326.0	0.1763	3158.04
s	0.15	0.35	60.0	0.5657	731.1	0.0371	3795.68
p	0.35	0.15	30.0	0.5622	1016.5	0.0897	3393.99
s	0.35	0.15	30.0	0.5622	667.3	0.0371	3464.45

Form Factor Summary:	P-Wave	S-Wave	All Cases
Mean	3345.49	3403.38	3374.43
Standard Deviation	195.22	282.42	244.49
Percent of Mean	5.83	8.30	7.24

Conclusions

We have shown the development of a new type of constitutive law for cemented granular material using statistical mechanics and based on the granular level characteristics of the assembly, such as bond damage (fracture) and topology. The distinct element method has provided a numerical testbed to evaluate the ability of the constitutive law to predict the effective elastic moduli of materials with widely varying degrees of damage and anisotropy. The results have shown that the analytic theory is in good agreement with the calculations, i.e. the variability in the predictions is of the same order as the variability of bond isotropy. The distinct element method has also been shown to provide valuable insight as to how the microscale fracture process can influence macroscopic failure in specific boundary value problems such as surface spall, compaction, and tensile strength. It is clear from this study that macroscopic inelasticity of quasi-brittle geologic materials, which traditionally has been modeled with plasticity formulations, may be better served by a constitutive law based on micromechanical considerations. One such model has been described in this paper.

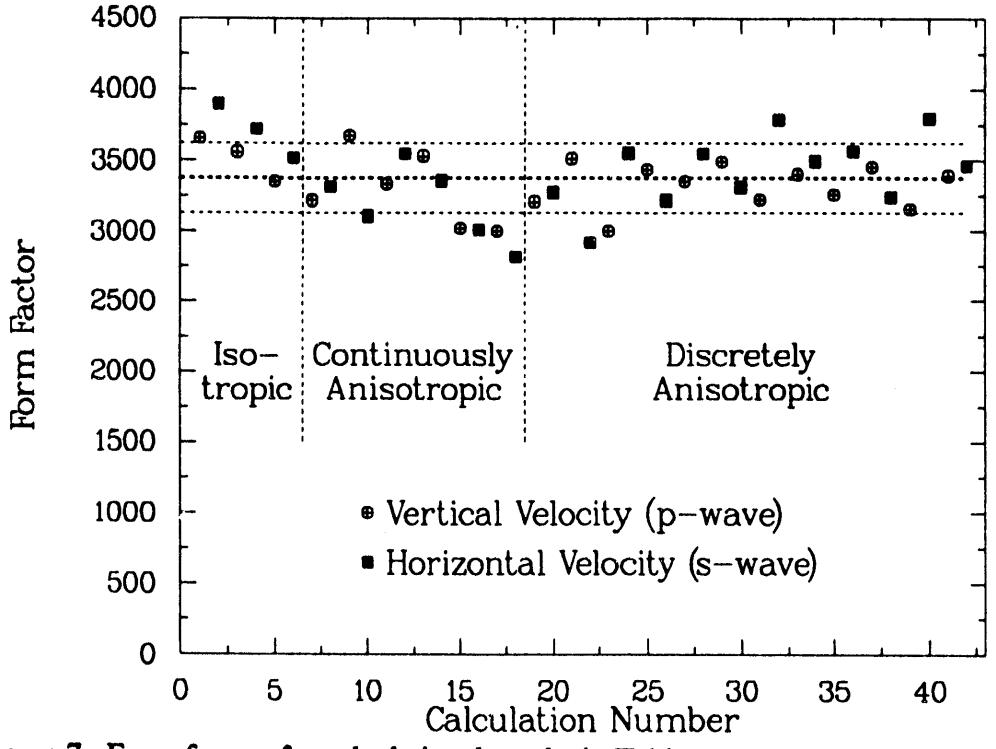

Figure 7. Form factors for calculational results in Tables 1 and 2 for an assembly of 1042 particles and 2906 bonds. The thick dashed line is the mean value for all cases and one standard deviation is also indicated. The overall mean is 3374.4 with a standard deviation of 7.2%.

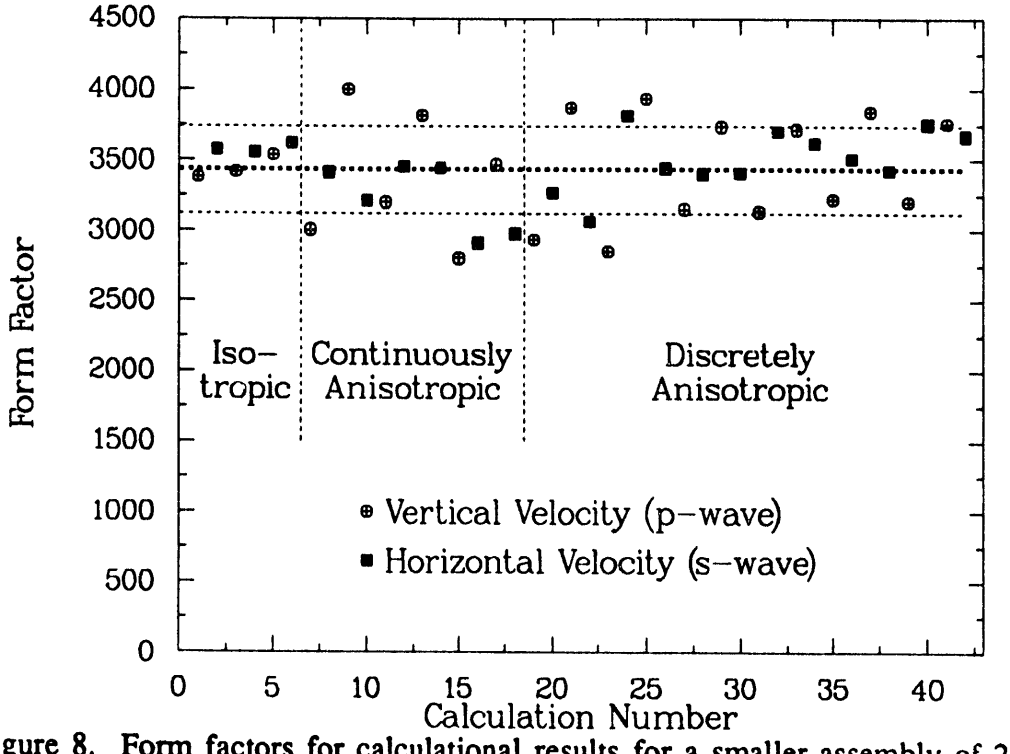

Figure 8. Form factors for calculational results for a smaller assembly of 270 particles and 610 bonds. Here the mean is 3477.9 with a standard deviation of 8.8%.

REFERENCES

P.A. Cundall, 1987, "Distinct element models of rock and soil structures," Proc. Analytic and Computational Methods in Engineering Rock Mechanics, E.T. Brown, Ed., A. Unwine Publishers, London, pp129-163 (1987).

A.A. Griffith, 1920, "Phenomena of rupture and flow in solids," Phil. Trans. R. Soc. A221, pp 163-198.

L.G. Margolin, 1984a, "Microphysical models for inelastic material response," Int. J. Eng. 22, 1171-1179.

L.G. Margolin, 1984b, "Generalized Griffith criteria for crack propagation," Int. J. Fracture 22, 65-69.

L.G. Margolin and B.C. Trent, 1990, "Towards a constitutive model for cemented granular materials, Proc. 31st U.S. Symposium on Rock Mechanics, W.A. Hustrulid and G.A. Johnson, Eds. Colorado School of Mines, Golden, Colorado, pp 321-328.

L.G. Margolin and B.C. Trent, 1992, "Towards a constitutive model for cemented granular materials II, Proc. 33st U.S. Symposium on Rock Mechanics, J.R. Tillerson and W.R. Wawersik, Eds., Santa Fe, NM, pp 671-679.

B.C. Trent, 1987, "The effect of micro-structure on the macroscopic behavior of a cemented granular material," Ph.D. Thesis, University of Minnesota (1987).

B.C. Trent, 1988, "Microstructural effects in static and dynamic numerical experiments," Proc. 29th U.S. Symposium on Rock Mechanics, Minneapolis, MN, pp 395-402.

B.C. Trent and L.G. Margolin, 1992a, "A numerical laboratory for granular solids," Engineering Computations 9, pp. 191-197.

B.C. Trent and L.G. Margolin, 1992b, "Numerical validation of a constitutive theory for an arbitrarily fractured solid, Proc. 2nd International Conference on Discrete Element Methods, March 17-18, at Massachusetts Institute of Technology.

Acknowledgments

This work was performed under the auspices of the U.S. Department of Energy by Los Alamos National Laboratory. LGM was supported by the Institute for Geophysics and Planetary Physics. BCT acknowledges the support of the Applied Theoretical Physics Division and Dynamic Experimentation Division at Los Alamos National Laboratory.

Appendix - Solutions of Angular Integrals in Consititutive Law

The summation term inside the angular brackets on the left side of Eq. 8 can be expressed as the following integrals if it is assumed that the bonds as well as any damage are isotropically distributed:

$$< \sum_{a=1}^{N_a} \tau_i^{(a)} \tau_j^{(a)} \tau_k^{(a)} \tau_m^{(a)} \left(\alpha^{(a)} - \beta^{(a)} \right) > = \int_0^{\frac{\pi}{2}} \sin^4\theta \, [\alpha(\theta) - \beta(\theta)] \, d\theta \qquad \text{(a1)}$$

for longitudinal (p-wave) loading and

$$< \sum_{a=1}^{N_a} \tau_i^{(a)} \tau_j^{(a)} \tau_k^{(a)} \tau_m^{(a)} \left(\alpha^{(a)} - \beta^{(a)} \right) > = \int_0^{\frac{\pi}{2}} \sin^2\theta \, \cos^2\theta \, [\alpha(\theta) - \beta(\theta)] \, d\theta \qquad \text{(a2)}$$

for shear (s-wave) loading.

Case 1 Solutions

If α is assumed constant and $\beta(\theta)$ is given as in Eq. 9, then, for $\phi=0$, the solution of Eq. (a1) can be evaluated as

$$\int_0^{\frac{\pi}{2}} \sin^4\theta \left[\alpha - \left\{ \beta_0 + \beta_1 \cos^2(\theta) \right\} \right] d\theta = (\alpha - \beta_0) \left(\frac{3\pi}{16} \right) - \beta_1 \left(\frac{\pi}{32} \right) \qquad \text{(a3)}$$

and for $\phi=\pi/2$, Eq. (a1) can be written as

$$\int_0^{\frac{\pi}{2}} \sin^4\theta \left[\alpha - \left\{ \beta_0 + \beta_1 \cos^2\left(\theta + \frac{\pi}{2} \right) \right\} \right] d\theta = (\alpha - \beta_0) \left(\frac{3\pi}{16} \right) - \beta_1 \left(\frac{5\pi}{32} \right) \qquad \text{(a4)}$$

These expressions are evaluated for the assumed values of α, β_0 and β_1 and appear in Table 1. For the shear wave loading, Eq. (a2) can be written as

$$\int_0^{\frac{\pi}{2}} \sin^2\theta \, \cos^2\theta \left[\alpha - \left\{ \beta_0 + \beta_1 \cos^2(\theta) \right\} \right] d\theta = (\alpha - \beta_0) \left(\frac{\pi}{16} \right) - \beta_1 \left(\frac{\pi}{32} \right) \qquad \text{(a5)}$$

for $\phi=0$. The solution of Eq. (a2) is identical for the case of $\phi=\pi/2$. Again, these are evaluated for the chosen values of α, β_0 and β_1 and then appear in Table 1.

Case 2 Solutions

Again, if α is assumed constant and $\beta(\theta)$ is given now as in Eq. 10, then for p-wave loading, Eq. (a1) can be expressed for any value of ϕ as

$$\int_0^{\phi} \sin^4\theta\,(\alpha - \beta_1)d\theta + \int_{\phi}^{\frac{\pi}{2}} \sin^4\theta\,(\alpha - \beta_0)d\theta \qquad \text{(a6)}$$

and the solution for any value of the damage separation angle, ϕ, is

$$(\alpha-\beta_0)\frac{3\pi}{16} + (\beta_1-\beta_0)\left[\frac{3\phi}{8} + \frac{\sin 2\phi}{4} + \frac{\sin 4\phi}{32}\right] \qquad \text{(a7)}$$

This expression is evaluated for the values of α, β_0, β_1 and ϕ chosen for the distinct element analysis, and are listed in Table 2. For the shear wave loading, Eq. (a2) can be expressed as

$$\int_0^{\phi} \sin^2\theta\,\cos^2\theta\,(\alpha - \beta_1)d\theta + \int_{\phi}^{\frac{\pi}{2}} \sin^2\theta\,\cos^2\theta\,(\alpha - \beta_0)d\theta \qquad \text{(a8)}$$

The solution for any value of the damage separation angle, ϕ, is

$$(\alpha-\beta_0)\left[\frac{\pi}{16} - \frac{\phi}{8} + \frac{\sin 4\phi}{32}\right] + (\alpha-\beta_1)\left[\frac{\phi}{8} - \frac{\sin 4\phi}{32}\right]. \qquad \text{(a9)}$$

This expression was evaluated for the specified values of α, β_0, β_1 and ϕ, and used to evaluate the form factors in Table 2.

DATE
FILMED
9/8/94

END